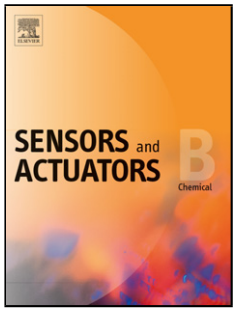

Title: Protein templated Au-Pt nanoclusters-graphene nanoribbons as a high performance sensing layer for the electrochemical determination of diazinon

Authors: Niyoosha Pajooheshpour, Mosayeb Rezaei, Ali Hajian, Abbas Afkhami, Mika Sillanpää, Fabiana Arduini, Hasan Bagheri

PII: S0925-4005(18)31441-2
DOI: https://doi.org/10.1016/j.snb.2018.08.014
Reference: SNB 25161

To appear in: *Sensors and Actuators B*

Received date: 29-5-2018
Revised date: 30-7-2018
Accepted date: 3-8-2018

Please cite this article as: Pajooheshpour N, Rezaei M, Hajian A, Afkhami A, Sillanpää M, Arduini F, Bagheri H, Protein templated Au-Pt nanoclusters-graphene nanoribbons as a high performance sensing layer for the electrochemical determination of diazinon, *Sensors and amp; Actuators: B. Chemical* (2018), https://doi.org/10.1016/j.snb.2018.08.014

Protein templated Au-Pt nanoclusters-graphene nanoribbons as a high performance sensing layer for the electrochemical determination of diazinon

Niyoosha Pajooheshpour [a], Mosayeb Rezaei [b], Ali Hajian [c], Abbas Afkhami [d], Mika Sillanpää [e,], Fabiana Arduini [f], Hasan Bagheri [g,*]

[a] *Faculty of Pharmaceutical Chemistry, Pharmaceutical Sciences Branch, Islamic Azad University, Tehran, Iran*

[b] *Young Researchers and Elite Club, Hamedan Branch Islamic Azad University, Hamedan, Iran*

[c] *Institute of Sensor and Actuator Systems, TU Wien, 1040 Vienna, Austria*

[d] *Faculty of Chemistry, Bu-Ali Sina University, Hamedan, Iran*

[e] *Laboratory of Green Chemistry, School of Engineering Science, Lappeenranta University of Technology, Sammonkatu 12, FI-50130, Mikkeli, Finland*

[f] *Department of Chemical Science and Technologies, University of Rome Tor Vergata, Via della Ricerca Scientifica, 00133 Rome, Italy*

[g] *Chemical Injuries Research Center, Systems Biology and Poisonings Institute, Baqiyatallah University of Medical Sciences, Tehran, Iran*

* Corresponding author. Tel.: +98 21 82482000; Fax: +98 21 82482000.
E-mail address: h.bagheri82@gmail.com; h.bagheri@bmsu.ac.ir (Hasan Bagheri).

Graphical abstract

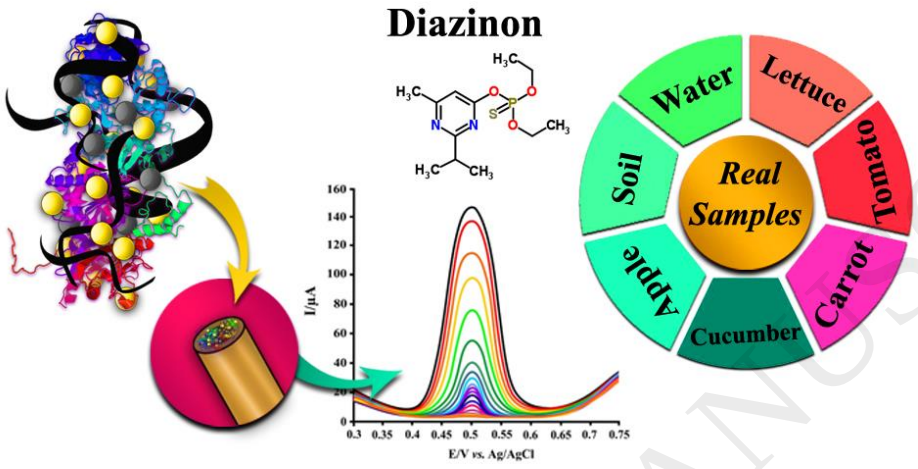

Highlights

- Enzymeless detection of diazinon based on Au-Pt nanoclusters-graphene modified sensor
- Direct and ultrasensitive electrochemical detection of diazinon at 0.50 V *vs.* Ag/AgCl.
- The sensor was utilized for detection of diazinon in water, fruit and vegetable samples

ABSTRACT

A new sensing layer composed of BSA templated Au-Pt bimetallic nanoclusters (Au-Pt@BSA/GCE) and graphene nanoribbons (GNRs) was employed for the rapid, selective and

sensitive determination of diazinon as an enzyme-less electrochemical sensor. The UV-Visible absorption spectroscopy, fluorescence spectroscopy, transmission electronic microscopy, X-ray diffraction and Fourier transform infrared techniques were used to investigate the size, morphology, and structure of the synthesized nanocomposite. Additionally, the electrochemical properties of the sensor were investigated by cyclic voltammetry, square wave anodic stripping voltammetry and electrochemical impedance spectroscopy. The results showed that Au-Pt@BSA-GNRs/GCE significantly catalyzes the oxidation and reduction of diazinon during electrochemical detection. The linear ranges of diazinon were between 0.01 to 10.0 and 10.0 to 170 µM, with a detection limit of 0.002 µM. The selectivity, stability, and reproducibility of Au-Pt@BSA-GNRs/GCE were studied, and obtained data indicates the great potential of the sensor as an alternative to enzyme inhibition-based biosensors for the determination of diazinon. The constructed electrode was employed for the determination of diazinon in some real samples with complex matrices such as soil, diverse water, fruit, and vegetables. The results indicate the excellent capability of the method for the detection of diazinon in real samples in comparison with the standard method.

Keywords:

Electrochemical sensors; Graphene nanoribbon; Organophosphates detection; Protein nanoclusters; Diazinon; Enzyme-less sensor.

1. Introduction

Organophosphorus (OP) pesticides are compounds widely used in agri-food sector for their lower persistence in the environment in respect to organochlorine pesticides but with high toxicity. In fact, they have the capability to inhibit in an irreversible way a key enzyme of nervous transmission i.e. acetylcholinesterase enzyme. with the accumulation of acetylcholine neurotransmitter leading often to death [1]. Among several organophosphorus pesticides, diazinon is as an organophosphorus pesticide which contains a thiophosphate ester together with the phosphorus center [2]. The proposed mechanism claims that sulfur is protonated in acidic medium via a hydronium ion, which ultimately delivers a hydroxide group to the phosphorus center and can react readily [2].

The wide use of diazinon in agricultural practices associated with their capability to moves freely with water percolating downward through the soil, renders this pesticide able to contaminate not only soil and surface water but even groundwater [3]. In addition, since diazinon exposure, whether from ingestion, skin contact, or inhalation causes severe symptoms such runny nose, drooling, loss of appetite, coughing, urination, diarrhea, stomach pain, and vomiting or even coma, the development of an effective and fast method for its detection is a crucial issue [4].

Some methods such as high-performance liquid chromatography (HPLC) [5], fluorescence [6], gas chromatography-mass spectroscopy (GC-MS) [7], surface enhanced Raman scattering (SERS) [8] and chemiluminescence techniques [9] have, however, been used for OPs compound detection over in recent decades, these techniques are often expensive, complex, time-consuming, and difficult to handle [10] and so a reliable method is needed to solve some common problems. Electrochemical methods have been found as a highly-sensitive, convenient and effective tool for

the analysis of important molecules and biomolecules including active ingredients in aqueous solution, pharmaceutical formulations and human body fluids [11-20]. Electrochemical methods in the analytical analysis may provide an effective answer with high selectivity and sensitivity to detect OP pesticides in environmental samples [21-23]. Up to now, most of the electrochemical sensors have been modified with metal nanomaterials [24, 25] that provide some special functions, such as catalytic and conductivity properties and the roughening of the conductive sensing interface [26].

Among nanomaterials, gold nanoparticles and especially gold nanoclusters (Au NCs) [27] have received considerable attention due to their strong surface plasmon (SP) absorption band, high conductivity and a larger number of available electro-active sites to detect analytes with improved sensitivity and low detection limit by minimizing the diffusion distance of analytes at the electrode surface [27-30]. NCs that are generally less than 10 nm in diameter have generated intense interest over the past decade. One reason for this is the belief that NCs will have unique properties, derived in part from the fact that these particles and their properties lie somewhere between those of bulk and single-particle species. NCs also have significant potential as new types of higher activity and selectivity catalysts. Two reasons chemists believe that nanoclusters hold the potential to be more active and selective catalysts than those of today are that a large percentage of a NC's metal atoms lie on the surface, and that surface atoms do not necessarily order themselves in the same way that those in the bulk do. Furthermore, the electrons in a nanocluster are confined to spaces that can be as small as a few atom-widths across, giving rise to quantum size effects [27, 28].

The combination of the metallic nanoclusters with another metal is one of the common ways of increasing the favorite characteristics and thermodynamic stability of the metallic

nanoclusters. Platinum nanoclusters (Pt NCs) combined with Au NCs are expected to strengthen adsorption ability as well as to improve stability, sensitivity, excellent electron transfer speed, and conductivity. These characteristics make them the ideal modifier on the surface of solid electrodes for different uses in the field of biomedical and environmental science [31].

In the past decade, efforts have been made with regard to design facile synthesis of Au-Pt nanoclusters using different approaches with the increased use of biomolecules, such as enzyme, peptide, and oligonucleotide, as environmentally favored templates. Among templates, bovine serum albumin (BSA)-protected Au or Pt NCs have some fascinating features, including easiness of synthesis, , excellent biocompatibility, stability, and surface functionality, which also makes them excellent candidates for immunoassays [32]. Since BSA has several types of functional groups, such as COOH, SH and NH, and a large amount of tyrosine and cysteine, it is one of the best candidates for the preparation of nanoclusters. Also, the BSA has the good biocompatibility and considerable cost advantages besides that it facilitated post-synthesis surface modifications with functional materials such as graphene.

Graphene (Gr) is a 2D atomic-scale honeycomb lattice made of carbon and, as monolayers graphite, have been used in varied instruments and especially in electronic devices to significantly improve performance [33]. This is due to the particular properties of Gr, such as an extremely large surface area (between 2,000-3,000 m^2 g^{-1}), high conductivity (about 105 to 106 S m^{-1}) and unprecedented mechanical, optical, thermal and magnetic traits [34, 35]. When the edges of the structure in Gr increase, some new electronic characteristics can be expected and this phenomenon happens when the size of Gr nanoplatelets is reduced to a few nanometers [36].

GNRs are tapes of Gr nanosheets (narrow and straight-edged stripes) with a width less than 50 nm, which have exceptional electronic properties [37]. Because of the ribbon structure of

GNRs, they have the properties of both multiwall carbon nanotubes (MWCNTs) and Gr. A recent report indicated that the area-normalized edge plane structures and chemically active sites of GNRs are much more than Gr and MWCNTs [36].

The main purpose of this study is to design an enzyme-less sensor to detect of diazinon, as a model of OP compounds using a green, simple and a cost-effective strategy to synthesize a sensing layer including protein-capped bimetallic Au-Pt nanoclusters and GNRs with good electrochemical properties. This methodology has excellent biocompatibility and considerable highly environmentally friendly properties. Moreover, the BSA coating layer on the Au-Pt nanoclusters facilitates post-synthesis surface modifications with functional materials. In this study, the direct electrochemistry of the composition of GNRs and protein-templated Au-Pt bi-metallic nanoclusters and their high electrocatalytic property in terms of diazinon sensing was investigated. The fabricated sensor exhibited excellent sensitivity, acceptable stability, fast response, and high electrocatalytic activity in the oxidation and reduction of diazinon.

2. Experimental

2.1. Chemicals and instrumentations

$HAuCl_4.3H_2O$, H_2PtCl_6, NaOH, BSA, MWCNTs, $KMnO_4$ and Diazinon were purchased from Merck Company (Germany) and used as received. Ultrapure water was used for the preparation of solutions. Britton–Robinson universal buffer solution (BRS, 0.04 M boric acid, 0.04 M acetic acid and 0.04 M phosphoric acid) with different pHs served as supporting electrolytes. Laboratory glassware was kept overnight in an HNO_3 solution (10% v/v) and was washed with ultrapure water before use.

Transmission electron microscope (TEM) images were taken using a Zeiss EM902A (Germany). Fourier transform infrared spectroscopy (FT-IR) spectra were obtained by a Perkin-

Elmer spectrophotometer (Spectrum GX). XRD patterns were determined by an XRD (38066 Riva, d/G.Via M. Misone, 11/D (TN) Italy) at ambient temperature. All of the electrochemical experiments were performed by an Ivium Vertex potentiostat/galvanostat system (Netherland). The electrochemical cell was assembled with a conventional three-electrode system consisting of an Ag/AgCl/KCl (3 M) electrode, platinum wire and modified/unmodified GCE employed as a reference electrode, auxiliary electrode and working electrode. Additionally, a Metrohm pH meter (model 713-Switzerland) with a combined pH glass electrode was used to determine pH values of the solutions. UV-Vis absorption and luminescence measurements were performed by an Agilent 8453 UV-Vis diode array spectrophotometer (Agilent, USA) and Perkin Elmer (LS50B) luminescence spectrometer, respectively.

2.2. Synthesis of the modifiers

Au-Pt@BSA was synthesized at 1:1 molar ratio of Au and Pt while BSA was used as a protecting and reducing agent. In the first step, 5.0 mL of a 10 mM $HAuCl_4$ aqueous solution (0.05 mmol Au) and 5.0 mL of a 10.0 mM H_2PtCl_6 (0.05 mmol Pt) were added to 5.0 mL of a 50 mg/mL BSA aqueous solution. In the second step, the previous mixture was continuously stirred at room temperature, and after 10 minutes 5.0 mL of 100 mM NaOH was immediately added to the mixture. The mixture was then stirred for 20 min at 70°C. In the final step, the solution was cooled to room temperature and dialyzed against ultrapure water for 24 h to remove all the free Au and Pt ions from the solution and obtain pure Au-Pt@BSA (Scheme 1a) [38]. Thereafter, Au-Pt@BSA bi-metallic nanoclusters were freeze-dried to obtain a solid powder for characterization and investigation. The other modifiers, including Pt@BSA and Au@BSA mono-metallic nanoclusters, were synthesized by the same method without the addition of $HAuCl_4$ and H_2PtCl_6, respectively [39].

GNRs was synthesized from MWCNTs using the method of Chiang et al. [40]. In this process, 0.2 g of MWCNTs was dispersed in 20 mL of concentrated sulfuric acid, then, 2 g KNO_3 was added to the mixture and it was stirred for 120 min at 400 rpm. In this step, a visually homogeneous black solution was obtained, then $KMnO_4$ was added to the previous solution and stirred for 120 min at ambient temperature. After that, the temperature was increased gradually up to 70 °C and kept at the same temperature until the reaction was complete (about 120 min in a water bath). Finally, the obtained mixture was cooled to ambient temperature, poured into 350 g of ice containing 5 mL of 35 % (v/v) H_2O_2 and then centrifuged until GNR solid was obtained. The resulting solid was removed then bath-sonicated in 60 mL of ultrapure water for 50 min, then bath-sonicated with the addition of 30 mL HCl. In the final step, the obtained product was centrifuged for 30 min and the collected solid was dispersed in 100 mL ether for 60 min. The suspension was centrifuged and purified GNRs were collected for use in the electrode matrix (Scheme 1a) [35].

For the synthesis of Au-Pt@BSA-GNRs, Au@BSA-GNRs, Pt@BSA-GNRs and BSA-GNRs nanocomposite, 0.4 mg of GNRs was added to 10 mL of Au-Pt@BSA, Au@BSA, Pt@BSA, and BSA, respectively, kept sonicating for 45 min and then centrifuged. The obtained participate was the desired nanocomposite (Scheme 1a).

2.3. Fabrication of electrochemical sensor

Before using GCE as the unmodified electrode and platform for the placement of the modifiers, it was polished to a mirror-like surface with 0.05 mm of alumina powder and immersed in HCl (37% w/w). It was then washed in an ultrasonic bath for 10 min, and finally, the prepared GCE was finally dried under nitrogen for subsequent use. For the preparation of Au-Pt@BSA-GNRs/GCE, Au@BSA-GNRs/GCE, Pt@BSA-GNRs/GCE, BSA-GNRs/GCE and BSA /GCE, 10

µl of Au-Pt@BSA-GNRs, Au@BSA-GNRs, Pt@BSA-GNRs, BSA-GNRs or a BSA suspension was cast on the surface of the prepared GCE and dried at ambient temperature (Scheme 1b).

Scheme 1

2.4. Electrochemical measurement procedure

The three electrodes were placed in an electrochemical cell containing a buffer solution, and the desired concentration of diazinon with the pH adjusted to 2.0 was constantly stirred with exposure to gaseous high-purity N_2 for 5 min to remove the dissolved oxygen. Before determination, N_2 was stopped, and the measurement procedure was started with the following steps. In the first step, diazinon accumulation was performed at -0.10 V *vs.* Ag/AgCl for 130 s. After that, stirring was stopped and a resting time of 10 s was applied to decrease the background current. In the second step, square wave voltammograms (SWV), one of the best analytical techniques, was carried out in a positive potential direction from 0.30 to 0.75 V *vs.* Ag/AgCl.

2.5 Preparation of the real samples

This section is described in detail in the section Supplementary Information.

3. Results and discussion

3.1. Characterization of the synthesized Au-Pt@BSA and GNRs

To investigate the composition of the synthesized Au-Pt@BSA and GNR nanocomposite, different methods such as UV-visible, fluorescence, TEM, XRD, and FT-IR were employed. The UV-visible absorption spectrum of the Au-Pt@BSA only shows a peak at 276 nm in the range of 250-650 nm which is related to the absorption of BSA biomolecules (Fig. 1a). Since no peak at 550 nm is observed, it can be concluded that highly purified Au-Pt@BSA NCs have been synthesized [39].

The fluorescence spectra of the prepared BSA, Au@BSA, Pt@BSA, and Au-Pt@BSA NCs are presented in Fig. 1b. BSA shows a broad fluorescent emission peak at 410 nm. Meanwhile, the fluorescence spectra of Au@BSA and Au-Pt@BSA NCs show that two peaks occur at about 404 and 640 nm. On the other hand, Pt@BSA had a fluorescent emission peak at approximately 407 nm, which the intensity is much lower than Au@BSA and Au-Pt@BSA NCs. It can be seen that the intensity of both peaks for Au@BSA NCs is equal, while this ratio is 2:1 (Intensity in 404:640 nm) for Au-Pt@BSA NCs. Also, the intensity in 404 nm for Au-Pt@BSA NCs is more than Au@BSA NCs due to the simultaneous formation of Au and Pt NCs onto BSA and improvement in the structural rigidity of BSA and the synergistic effect between Au NCs and Pt NCs for BSA. Furthermore, the increase in the intensity of the signal and peak shift to a lower wavelength for Au-Pt@BSA NCs can be attributed to the synergistic effect of Au and Pt NCs and confirm the formation of Au-Pt@BSA [39].

Fig. 1

Fig. 1c shows the XRD diffraction patterns of BSA and the synthesized Au@BSA, Pt@BSA and Au-Pt@BSA nanocomposites. The XRD patterns of BSA clearly show a typical characteristic peak that matches well with the reported patterns [41]. The XRD patterns of Au@BSA and Pt@BSA confirmed the formation of the monometallic phase of Au (JCPDS 04-1784) [42] and Pt (JCPDS 05-0681) [43] on BSA with high crystallinity. No impurity peaks of Au and Pt NCs were observed, which indicates the high purity of Au@BSA and Pt@BSA NCs. In addition, peaks of the Au-Pt@BSA nanocomposite appeared at 2θ of 39.37° (111), 40.88° (111), 45.52° (200), 47.07° (200), 65.83° (220), 68.69° (220), 79.02° (311), and 68.73° (311), suggesting the formation of BSA-loaded Au and Pt NCs.

The FT-IR spectra confirm the formation of the synthesized nanocomposites and the results are shown in Fig. 1d. The figure shows that the FT-IR spectrum of free BSA has clear absorption bands at approximately 3432, 3065, 1678 and 1526 cm^{-1}, which confirm the presence of O-H, NH, and amide I and amide II stretching vibrations, respectively [44]. The FT-IR spectra of Au@BSA and Pt@BSA were closely analogous to each other and to the Au-Pt@BSA spectrum. The spectrum of Au-Pt@BSA shows a significant shift of amide I to a lower wave number (1,678 to 1,637 cm^{-1}) and a small shift of amide II to a higher wave number (1,526 to 1,555 cm^{-1}), which demonstrates the secondary structure change of BSA and the loading of Au and Pt nanoclusters onto BSA. Also, the all specific absorption bands of Au-Pt@BSA and GNRs in FT-IR of Au-Pt@BSA-GNRs exist [45].

The morphology of the prepared Au-Pt@BSA nanocomposite was examined by TEM. Fig. 2a shows the formation of the core-shell-like structure of Au-Pt nanoclusters with an average size of approximately 2.25±0.18 nm. The EDX spectrum of Au-Pt@BSA nanocomposite is shown in Fig. 2b and exhibits the presence of Au, Pt, C, O, N, S, and Cl elements, which confirm the presence of the Au and Pt NCs in the BSA.

Fig. 2

Also, the FT-IR spectra and XRD pattern of MWCNTs and GNRs are presented and described in detail in the Supplementary information (Figs. S1 and S2).

3.2. Electrochemical characterization of the sensor

Fig. 3a shows the CVs of the bare GCE, BSA/GCE, BSA-GNRs/GCE and Au@ BSA-GNRs/GCE, Pt@BSA-GNRs/GCE and Au-Pt@BSA-GNRs/GCE using a solution of 5.0 mM $[Fe(CN)_6]^{3-/4-}$ in 1.0 M KCl. The bare GCE (curve a) shows a pair of broad and weak redox peaks with a peak separation (ΔE_p) of 266 mV, but the BSA/GCE significantly blocks the redox response

with increases of ΔE_p of 349 mV. Once the GNRs were added to the BSA, the peak separation has decreased (ΔE_p=219) with a remarkable increase in the redox currents in comparison with BSA/GCE and GCE. However, the electron-transfer reaction of ferricyanide improved because the GNRs increased the conductivity of BSA/GCE.

On Au@BSA-GNRs/GCE and Pt@BSA-GNRs/GCE, a pair of well-defined peaks appeared with a lower ΔE_p value and higher I_p, which was due to the increase of the conductivity of the electrodes as a result of the presence of the mono-metallic NCs. The Au-Pt@BSA-GNRs/GCE displayed a pair of well-defined peaks with the lowest ΔE_p value of 63 mV, and the I_{pa} of Au-Pt@BSA-GNRs/GCE was found to be 1.87, 3.02 and 1.50 times higher than those of bare GCE, BSA/GCE, and BSA-GNRs/GCE, respectively, which suggests that the modified electrodes have a faster electron transfer rate due to the synergic effects of Au, Pt, and GNRs.

For more study the transfer coefficient (α) and heterogeneous electron transfer rate constant (k_s) were calculated by plotting the potential of peaks *vs.* the logarithm of the sweep rate base on Laviron's equation (Eq. 1) [46] for Au-Pt@BSA-GNRs/GCE (Fig.3b).

$$E_{pc}=E^{o'}-[\frac{2.3RT}{\alpha nf}]\log(\frac{\alpha nf}{RT}\times\frac{v}{Ks}) \qquad \text{Eq. 1}$$

Based on the Laviron's equation (Eq. 1) α and k_s were measured 0.524 and 7.01 s^{-1}, respectively. The gained k_s for Au-Pt@BSA-GNRs/GCE is higher the obtained values for BSA/GCE (0.002 s^{-1}), BSA-GNRs/GCE (1.12 s^{-1}), Au@ BSA-GNRs/GCE (6.28 s^{-1}), and Pt@BSA-GNRs/GCE (6.13s^{-1}), which indicates the reasonably fast electron transfer of $Fe[(CN)_6]^{3-/4-}$ at Au-Pt@BSA-GNRs/GCE.

Electrochemical impedance spectroscopy (EIS) was employed to investigate the characteristics of the probe layers on the electrochemical sensors. In EIS, the semicircular part at

higher frequencies and linear part at lower frequencies correspond to the electron transfer resistance (R_{ct}) and limited diffusion process, respectively. The diameter of the semicircle equals R_{ct} represents the difficulty of electron transfer of a ferrocyanide -redox probe- between the solution and the electrode, supplying information of the electrochemical interphase [47]. Fig. 3c shows the EIS of the different electrodes. When bare GCE was modified by BSA, the diameter of the semicircle increased, suggesting that BSA insulated the surface of GCE and made an interfacial charge transfer inaccessible. The GNRs increased the conductivity of BSA/GCE and the R_{ct} value dropped significantly (209 Ω). Pt, Au and Pt-Au nanoclusters were then immobilized on BSA-GNRs/GCE, and the diameters of the semicircles were clearly lower than those of the other electrodes. The electron-transfer resistance values for Pt@BSA-GNRs/GCE, Au@BSA-GNRs/GCE, and Au-Pt@BSA-GNRs/GCE were 176, 165 and 122 Ω, respectively, indicating that the results indicated electron transfer rate was significantly increased due to the simultaneous presence of Au and Pt NCs on BSA and the utilization of GNRs. In addition, the CVs of the potassium ferrocyanide solution on bare GCE, BSA/GCE, BSA-GNRs/GCE, Pt@BSA-GNRs/GCE, Au@BSA-GNRs/GCE and Au-Pt@BSA-GNRs/GCE were analyzed with the aim of determining the electrochemically active surface areas by the Randles-Sevcik equation [47, 48]. The obtained electrochemical active surface area of bare GCE, BSA/GCE and BSA-GNRs/GCE were calculated as 0.0705, 0.0516 and 0.1299 cm^2, respectively. In addition, to investigate the effect of Au and Pt NCs, the electrochemical surface areas of Pt@BSA-GNRs/GCE, Au@BSA-GNRs/GCE were calculated as 0.268 and 0.277 cm^{-1}, respectively, which show the Au and Pt NCs increased the active surface of BSA-GNRs/GCE.

Fig. 3

The calculated surface area of Au-Pt@BSA-GNRs/GCE (0.3027 cm^2) was more than that of the other electrodes, due to the presence of Au and Pt nanoclusters as an effectual modifier that can supply an extensive surface area and improved electron transfer rate on the surface of the electrode. The roughness factors (ρ) were calculated for bare BSA/GCE, BSA-GNRs/GCE, Pt@BSA-GNRs/GCE, Au@BSA-GNRs/GCE and Au-Pt@BSA-GNRs/GCE base on the ratio of electrochemical surface area to the geometrical surface of the electrodes [49] and were found to be 0.732, 1.843, 3.801, 3.929 and 4.294, respectively. These computed roughness factor could be showed the effect of presence of the modifiers and the morphology of the working electrodes which demonstrating the increase of the electrode surface roughness in the presence of the nanoclusters and GNRs.

3.3. Electrochemical behavior of diazinon on the Au-Pt@BSA/GCE-GNRs

To investigate the electrochemical ability of the developed sensor, the SWVs of diazinon were recorded on the surfaces of various electrodes, and the results are shown in Fig. 4a. In all the experiments, pH, deposition potential, accumulation time, resting time, SW frequency, pulse amplitude, and voltage step were 2, -0.1 V *vs.* Ag/AgCl, 130 s, 10 s, 50 Hz, 100 mV and 6.0 mV, respectively.

As seen in Fig. 4a, no square wave anodic stripping peaks were observed in the potential range on the surface of bare GCE and BSA/GCE in the presence of 8.0 μM diazinon. The analyte has a broad peak with low oxidation current at the surface of BSA-GNRs/GCE. The BSA-GNRs/GCE modified with Pt nanocluster (Pt@BSA-GNRs/GCE) exhibited a clear oxidation peak corresponding to diazinon at approximately 0.50 V *vs.* Ag/AgCl and, once Au@BSA-GNRs/GCE is used as working electrode, the oxidation peak current is higher than with Pt@BSA-GNRs/GCE. The remarkable increase in the peak current of diazinon on the Au-Pt@BSA-GNRs/GCE can be

attributed to the excellent electrical conductivity and high surface area of the Au and Ag nanoclusters.

Fig. 4

These electrode reactions involved redox reactions in the diazinon. Although, gold and platinium were commonly used in heterogeneous catalytic redox of aromatic compounds to corresponding species in a very high yield and a very high chemoselectivity, there is no report elucidating the electrochemical behaviour of diazinon on the electrodes modified with Au- and Pt NCs. Based on the above-obtained results, it can be say that Au-Pt@BSA/GCE with greatly improving oxidation current, the sensitivity and detection limit can be ameliorate compared to the other electrodes. In addition, the SWV experiments proven that Au-Pt@BSA-GNRs /GCE showed good electro-catalytic activity toward the oxidation of diazinon.

3.4. pH optimization

The experimental conditions have significant influence on the detection sensitivity of diazinon. As protons participate in this reaction at Au-Pt@BSA-GNRs/GCE, the acidity of buffer buffer has a remarkable effect on the electrochemical behavior of diazinon [50, 51]. Therefore, the effect of pH was studied over the range of 1.0-8.0 with BRS. Fig. 4b shows the SWASV of 8.0 µM diazinon using the developed sensor at different pHs. At first, the current response increased and reached to the maximum at pH 2.0, then declined significantly along with the increase of buffer pH (Fig. 4c). At pH=1.0, the decrease in current may be due to the fast acid hydrolysis of the P-O-C=N because of the protonation of the nitrogen atom on the heterocyclic ring [50]. Meanwhile, with the increase of pH, the peak potential shifted negatively and showed linear relationship with pH values from 1.0 to 8.0 (Fig. 4d). The linear regression equation between the pH and oxidation

peak potential for diazinon was E=-0.0562 pH + 0.609 (R^2 = 0.9937). According to the following equation:

E_p=K-(0.059) m/n pH Eq. 2

where *m* and *n* refer to the transferring number of protons and electrons, respectively. The value of obtained slope value was equal approximately to the theoretical value, indicating that the transferring number of protons and electrons were equal, which was in good accordance with the literatures reported (two electrons and two protons) [50].

3.5. Effect of the deposition potential, and accumulation time

The effect of the deposition potential on the stripping current of 8.0 µM diazinon was studied in the range of +300 to -400 mV *vs.* Ag/AgCl on Au-Pt@BSA-GNRs/GCE. The results are shown in Fig. 4e. The highest response was obtained at a deposition potential of -100 mv *vs.* Ag/ AgCl while deposition time was 132 s.

The effect of accumulation time on the voltammetric stripping currents of 8.0 µM diazinon was studied from 0 to 200 s on Au-Pt@BSA-GNRs/GCE, and the results are shown in Fig. 4f. It was found that the voltammetric stripping currents for diazinon rise as time passes, and after 130 s, the anodic stripping current becomes almost constant as a result of the sensor's surface saturation [52, 53]. Therefore, an accumulation time of 130 s and deposition potential of 100 mV were used in all further studies. The result of the optimized instrumental parameters is shown in Table S1.

3.6. Determination of diazinon on Au-Pt@BSA-GNRs/GCE

As shown in Fig. 5a and b, the corresponding anodic stripping currents of diazinon increased in two linear regions in the concentration ranges of 0.01 to 10.0 and 10.0 to 170 µM. The relation between I_{pa} and the concentration of the analyte can be described by the below equations:

I_{pa} = 2.364C + 0.5385 R^2 = 0.9987 (0.01 to 10.0 µM) Eq. 3

I_{pa} = 0.7302C + 16.361 R^2 = 0.9990 (10.0 to 170 µM) Eq. 4

The limit of detection was estimated to be 0.002 µM based on the $3S_b/m$, where S_b is the standard deviation of the mean value of 10 independent SWASVs of the blank solution and m is slope of the first linear calibration range.

Fig. 5

3.7. The selectivity, stability, and reproducibility of Au-Pt@BSA-GNRs/GCE

The development of an enzyme-less electrode has attracted considerable attention due to its simple, low fabrication cost, long term stability and good reproducibility which are the limitations of those enzymatic biosensors. However, the selectivity of the electrode sensor for target analyte is still great challenge. Possible interferences of the electrochemical determination of diazinon at Au-Pt@BSA-GNRs/GCE were investigated by the addition of various ions and molecules to BRS in the presence of 8.0 µM of the analyte. The basis for selecting a species as an interference was a change in oxidation current of more than ±5%. Common ions such as Na^+, K^+, Cl^-, Zn^{3+}, Tl^+, Pb^{2+}, Fe^{3+}, Cu^{2+}, Hg^2, Mg^{2+}, Al^{3+}, $H_2PO_4^-$, HPO_4^{2-}, SO_4^{2-}, CO_3^{2-}, NO_3^-, ClO_4^- and SCN^-, did not show any interference for the determination of diazinon. Due to the enzyme can be affected by different kind of contaminations such as heavy metals in environmental samples, which makes the direct determination of organophosphorous pesticides lack of selectivity and even leads to false positive results. Therefore, this enzyme-less sensor is highly recommended. In addition, the interference of some compounds such as methyl paraoxon, methyl parathion, fenitrothion, atrazine, dicloran, dimethoate, glucose, lactose, and sucrose on the voltammetric measurements

was examined. The obtained results indicate that a 150-fold excess of methyl paraoxon, p-nitrophenol and nitrobenzene, methyl parathion and fenitrothion and a 600-fold excess of glucose, lactose, and sucrose had no effect on the oxidation peak current of diazinon (Fig. S3). It was concluded the oxidation process of diazinon onto the Au-Pt nanoclusters-graphene nanoribbons lead to a good improvement in peak resolution. As seen in Fig. S3 voltammograms registered after making additions of 50 µM p-nitrophenol, nitrobenzene and methyl parathion, and 30 µM Zn^{3+}, Tl^{+}, Pb^{2+}, Fe^{3+}, $Cu^{2+}$and Hg^{2+} to 4.0 µM diazinon show that its peak potential and current remain practically inalterable (±5%). The peaks of p-nitrophenol, nitrobenzene and methyl parathion are separated enough from diazinon peak. No interference has been found in diazinon determination up to 65-fold excess of atrazine, dicloran, and dimethoate which indicates that the presence of these molecules does not change the oxidation current of diazinon by more than 5%. Also, sugars cause no interference, and this enzyme-less sensor can be used to detect diazinon residual in some fruit extracts and drinks. Therefore, no remarkable current change was observed upon addition of interfering species, demonstrating preferable selectivity of the sensor for diazinon determination. The results indicated that, the sensing layer exhibited a high adsorption and strong affinity toward diazinon even in presence of inorganic salts, nitroaromatic compounds and other pesticides, which commonly existed in real samples. It was found that, the nano-sized architectures and composition of protein template Au-Pt NCs play key roles in the sensing performance in real samples.

Further study of the stability and reproducibility of Au-Pt@BSA-GNRs/GCE for the detection of diazinon was investigated in a solution containing 4.0 µM of the target analyte. Ten electrodes were prepared by the same method on different days to evaluate the reproducibility of Au-Pt@BSA-GNRs/GCE for determination of the analyte under optimum conditions. The calculated relative standard deviations (RSDs) value was 4.4% for diazinon. To evaluate the

stability, a fabricated electrode was stored in BRS with pH=2.0 at 4°C when not in use for 6 days. The results of the measurement of the oxidation peak currents showed that there was no great decrease in the response of the electrode. The obtained data suggest that Au-Pt@BSA-GNRs/GCE has high reproducibility and excellent stability for the determination of diazinon.

3.8. Real sample analysis

The electrode was used for electrochemical determination of diazinon in wastewater, river water, tap water, soil, apple, cucumber, carrot, tomato and lettuce samples by the standard addition method. Real samples were prepared by standard methods, which are described in detail in the section Supplementary Information; [54, 55]. The results are shown in Table 1 which it can be observed that the percentage recovery of the sample solution was between 95.3% and 105.0%. The results are also compared with the standard HPLC method, which indicates the ability of the proposed method to detect diazinon in different real sample matrices.

Table 1.

4. Conclusion

In this study, in order to overcome the problems of enzyme-based electrochemical sensors, including the high cost and low stability of the enzyme, difficulty in obtaining a pure form of it, and short storage and usage lifetime of the sensor, a simple method for voltammetric determination of diazinon was suggested. Enzymeless electrochemical sensors based on nanomaterials have attracted much attention because of their low cost, sensitivity and remarkable stability under extensive environmental and industrial conditions. Since the electrochemical properties of nanomaterials are largely influenced by their shape and structural features. Thus, synthesizing

novel morphologies with enhanced electrochemical characteristic is yet another important task to accomplish. The synthesized novel sensing layer including protein templated Au-Pt nanoclusters-graphene nanoribbons not only demonstrated attractive structural features but were known to possess excellent electrochemical characteristics, which enabled development of reliable, sensitive, robust` and selective electrochemical sensor for diazinon. The developed senor demonstrated wide linear ranges and low detection limit based on its suggested signal measurement in comparison with the other reported electrochemical sensors (Table S2). . In addition, the developed sensor utilizes a novel and simple approach towards detection of toxic species like diazinon which is not only economically feasible but practical in terms of its electrochemical nature.

Acknowledgements

The authors would like to thank National Institute For Medical Research Development (NIMAD) for the financial support this work (Grant No. 963477).

Reference

[1] X. Wang, X. Qiao, Y. Ma, T. Zhao, Z. Xu, Simultaneous determination of nine trace organophosphorous pesticide residues in fruit samples using molecularly imprinted matrix solid-phase dispersion followed by gas chromatography, Journal of agricultural and food chemistry, 61(2013) 3821-7.

[2] M. Nabi, A. Tabrizi, Effect of diazinon on gonadotropins and testosterone levels in serum of male rat, IJBPAS, 4(2015) 1119-26.

[3] H. Shemer, K.G. Linden, Degradation and by-product formation of diazinon in water during UV and UV/H2O2 treatment, Journal of hazardous materials, 136(2006) 553-9.

[4] F.L. Edwards, P.B. Tchounwou, Environmental toxicology and health effects associated with methyl parathion exposure–a scientific review, International journal of environmental research and public health, 2(2005) 430-41.

[5] Y. Zhang, H.K. Lee, Determination of ultraviolet filters in environmental water samples by temperature-controlled ionic liquid dispersive liquid-phase microextraction, Journal of Chromatography A, 1271(2013) 56-61.

[6] X. Meng, J. Wei, X. Ren, J. Ren, F. Tang, A simple and sensitive fluorescence biosensor for detection of organophosphorus pesticides using H2O2-sensitive quantum dots/bi-enzyme, Biosensors and Bioelectronics, 47(2013) 402-7.

[7] J.L. Armstrong, R.L. Dills, J. Yu, M.G. Yost, R.A. Fenske, A sensitive LC-MS/MS method for measurement of organophosphorus pesticides and their oxygen analogs in air sampling matrices, Journal of Environmental Science and Health, Part B, 49(2014) 102-8.

[8] J. Wang, L. Kong, Z. Guo, J. Xu, J. Liu, Synthesis of novel decorated one-dimensional gold nanoparticle and its application in ultrasensitive detection of insecticide, Journal of Materials Chemistry, 20(2010) 5271-9.

[9] J. Wu, X. Fu, C. Xie, M. Yang, W. Fang, S. Gao, TiO2 nanoparticles-enhanced luminol chemiluminescence and its analytical applications in organophosphate pesticide imprinting, Sensors and Actuators B: Chemical, 160(2011) 511-6.

[10] M. Nousiainen, K. Peräkorpi, M. Sillanpää, Determination of gas-phase produced ethyl parathion and toluene 2, 4-diisocyanate by ion mobility spectrometry, gas chromatography and liquid chromatography, Talanta, 72(2007) 984-90.

[11] V. K Gupta, A. Nayak, S. Agarwal, B. Singhal, Recent advances on potentiometric membrane sensors for pharmaceutical analysis, Combinatorial chemistry & high throughput screening, 14(2011) 284-302.

[12] V.K. Gupta, B. Sethi, R. Sharma, S. Agarwal, A. Bharti, Mercury selective potentiometric sensor based on low rim functionalized thiacalix [4]-arene as a cationic receptor, Journal of Molecular Liquids, 177(2013) 114-8.

[13] V.K. Gupta, M. Ganjali, P. Norouzi, H. Khani, A. Nayak, S. Agarwal, Electrochemical analysis of some toxic metals by ion–selective electrodes, Critical Reviews in Analytical Chemistry, 41(2011) 282-313.

[14] S.K. Srivastava, V.K. Gupta, M.K. Dwivedi, S. Jain, Caesium PVC–crown (dibenzo-24-crown-8) based membrane sensor, Analytical Proceedings including Analytical Communications, Royal Society of Chemistry1995, pp. 21-3.

[15] V.K. Gupta, H. Karimi-Maleh, R. Sadegh, Simultaneous determination of hydroxylamine, phenol and sulfite in water and waste water samples using a voltammetric nanosensor, Int J Electrochem Sci, 10(2015) 303-16.

[16] V.K. Gupta, A.K. Singh, L.K. Kumawat, Thiazole Schiff base turn-on fluorescent chemosensor for Al3+ ion, Sensors and Actuators B: Chemical, 195(2014) 98-108.

[17] S.K. Srivastava, V.K. Gupta, S. Jain, PVC-based 2, 2, 2-cryptand sensor for zinc ions, Analytical chemistry, 68(1996) 1272-5.

[18] V.K. Gupta, S. Kumar, R. Singh, L. Singh, S. Shoora, B. Sethi, Cadmium (II) ion sensing through p-tert-butyl calix [6] arene based potentiometric sensor, Journal of Molecular Liquids, 195(2014) 65-8.

[19] M.L. Yola, V.K. Gupta, T. Eren, A.E. Şen, N. Atar, A novel electro analytical nanosensor based on graphene oxide/silver nanoparticles for simultaneous determination of quercetin and morin, Electrochimica Acta, 120(2014) 204-11.

[20] V.K. Gupta, N. Mergu, L.K. Kumawat, A.K. Singh, A reversible fluorescence "off–on–off" sensor for sequential detection of aluminum and acetate/fluoride ions, Talanta, 144(2015) 80-9.

[21] Y. Zeng, D. Yu, Y. Yu, T. Zhou, G. Shi, Differential pulse voltammetric determination of methyl parathion based on multiwalled carbon nanotubes–poly (acrylamide) nanocomposite film modified electrode, Journal of hazardous materials, 217(2012) 315-22.

[22] X. Chen, G. Wu, Z. Cai, M. Oyama, X. Chen, Advances in enzyme-free electrochemical sensors for hydrogen peroxide, glucose, and uric acid, Microchimica Acta, 181(2014) 689-705.

[23] S. Park, H. Boo, T.D. Chung, Electrochemical non-enzymatic glucose sensors, Analytica chimica acta, 556(2006) 46-57.

[24] T. Rahmani, A. Hajian, A. Afkhami, H. Bagheri, A novel and high performance enzyme-less sensing layer for electrochemical detection of methyl parathion based on BSA templated Au-Ag bimetallic nanoclusters, New Journal of Chemistry, (2018).

[25] Z. Qiu, J. Shu, D. Tang, Near-Infrared-to-Ultraviolet Light-Mediated Photoelectrochemical Aptasensing Platform for Cancer Biomarker Based on Core–Shell NaYF4: Yb, Tm@ TiO2 Upconversion Microrods, Analytical chemistry, 90(2017) 1021-8.

[26] C. Priya, G. Sivasankari, S.S. Narayanan, Electrochemical behavior of Azure A/gold nanoclusters modified electrode and its application as non-enzymatic hydrogen peroxide sensor, Colloids and Surfaces B: Biointerfaces, 97(2012) 90-6.

[27] Q. Zhou, Y. Lin, M. Xu, Z. Gao, H. Yang, D. Tang, Facile synthesis of enhanced fluorescent gold–silver bimetallic nanocluster and its application for highly sensitive detection of Inorganic pyrophosphatase activity, Analytical chemistry, 88(2016) 8886-92.

[28] J.D. Aiken III, R.G. Finke, A review of modern transition-metal nanoclusters: their synthesis, characterization, and applications in catalysis, Journal of Molecular Catalysis A: Chemical, 145(1999) 1-44.

[29] J. Shu, Z. Qiu, S. Lv, K. Zhang, D. Tang, Plasmonic Enhancement Coupling with Defect-Engineered TiO2–x: A Mode for Sensitive Photoelectrochemical Biosensing, Analytical chemistry, 90(2018) 2425-9.

[30] T. Rahmani, A. Hajian, A. Afkhami, H. Bagheri, A novel and high performance enzyme-less sensing layer for electrochemical detection of methyl parathion based on BSA templated Au–Ag bimetallic nanoclusters, New Journal of Chemistry, 42 (2018) 7213-7222.

[31] H. Kawasaki, H. Yamamoto, H. Fujimori, R. Arakawa, M. Inada, Y. Iwasaki, Surfactant-free solution synthesis of fluorescent platinum subnanoclusters, Chemical Communications, 46(2010) 3759-61.

[32] Y. Chang, Z. Zhang, J. Hao, W. Yang, J. Tang, BSA-stabilized Au clusters as peroxidase mimetic for colorimetric detection of Ag+, Sensors and Actuators B: Chemical, 232(2016) 692-7.

[33] S. Stankovich, D.A. Dikin, G.H. Dommett, K.M. Kohlhaas, E.J. Zimney, E.A. Stach, et al., Graphene-based composite materials, nature, 442(2006) 282.

[34] F. Tadayon, S. Vahed, H. Bagheri, Au-Pd/reduced graphene oxide composite as a new sensing layer for electrochemical determination of ascorbic acid, acetaminophen and tyrosine, Materials Science and Engineering: C, 68(2016) 805-13.

[35] P. Hashemi, H. Bagheri, A. Afkhami, S. Amidi, T. Madrakian, Graphene nanoribbon/FePt bimetallic nanoparticles/uric acid as a novel magnetic sensing layer of screen printed electrode for sensitive determination of ampyra, Talanta, 176(2018) 350-9.

[36] M. Fujita, K. Wakabayashi, K. Nakada, K. Kusakabe, Peculiar localized state at zigzag graphite edge, Journal of the Physical Society of Japan, 65(1996) 1920-3.

[37] R. Faccio, P.A. Denis, H. Pardo, C. Goyenola, A.W. Mombrú, Mechanical properties of graphene nanoribbons, Journal of Physics: Condensed Matter, 21(2009) 285304.

[38] S. Wang, S. Jin, S. Yang, S. Chen, Y. Song, J. Zhang, et al., Total structure determination of surface doping [Ag46Au24 (SR) 32](BPh4) 2 nanocluster and its structure-related catalytic property, Science advances, 1(2015) e1500441.

[39] S.-N. Ding, Y.-X. Guo, One-pot synthesis of dual-emitting BSA–Pt–Au bimetallic nanoclusters for fluorescence ratiometric detection of mercury ions and cysteine, Analytical Methods, 7(2015) 5787-93.

[40] Y.-S. Li, J.-L. Liao, S.-Y. Wang, W.-H. Chiang, Intercalation-assisted longitudinal unzipping of carbon nanotubes for green and scalable synthesis of graphene nanoribbons, Scientific reports, 6(2016) 22755.

[41] L. Li, W. Feng, P. Ji, Protein adsorption on functionalized multiwalled carbon nanotubes with amino-cyclodextrin, AIChE Journal, 57(2011) 3507-13.

[42] J. Zhang, Y. Yuan, Y. Wang, F. Sun, G. Liang, Z. Jiang, et al., Microwave-assisted synthesis of photoluminescent glutathione-capped Au/Ag nanoclusters: a unique sensor-on-a-nanoparticle for metal ions, anions, and small molecules, Nano Research, 8(2015) 2329-39.

[43] R.K. Petla, S. Vivekanandhan, M. Misra, A.K. Mohanty, N. Satyanarayana, Soybean (Glycine max) leaf extract based green synthesis of palladium nanoparticles, J Biomater Nanobiotechnol, 3(2012) 14-9.

[44] J. Tian, J. Liu, Z. Hu, X. Chen, Interaction of wogonin with bovine serum albumin, Bioorganic & medicinal chemistry, 13(2005) 4124-9.

[45] S. Govindaraju, S.R. Ankireddy, B. Viswanath, J. Kim, K. Yun, Fluorescent gold nanoclusters for selective detection of dopamine in cerebrospinal fluid, Scientific reports, 7(2017) 40298.

[46] H. Bagheri, E. Ranjbari, M. Amiri-Aref, A. Hajian, Y.H. Ardakani, S. Amidi, Modified fractal iron oxide magnetic nanostructure: A novel and high performance platform for redox protein immobilization, direct electrochemistry and bioelectrocatalysis application, Biosensors and Bioelectronics, 85(2016) 814-21.

[47] H. Bagheri, A. Afkhami, H. Khoshsafar, A. Hajian, A. Shahriyari, Protein capped Cu nanoclusters-SWCNT nanocomposite as a novel candidate of high performance platform for organophosphates enzymeless biosensor, Biosensors and Bioelectronics, 89(2017) 829-36.

[48] H. Bagheri, A. Afkhami, H. Khoshsafar, M. Rezaei, S.J. Sabounchei, M. Sarlakifar, Simultaneous electrochemical sensing of thallium, lead and mercury using a novel ionic liquid/graphene modified electrode, Analytica chimica acta, 870(2015) 56-66.

[49] A.J. Bard, L.R. Faulkner, Fundamentals and applications, Electrochemical Methods, 2(2001) 482.

[50] D. Guziejewski, S. Skrzypek, W. Ciesielski, Square wave adsorptive stripping voltammetric determination of diazinon in its insecticidal formulations, Environmental Monitoring and Assessment, 184(2012) 6575-82.

[51] R.C. Martinez, F.B. Dominguez, J.H. Mendez, P.G. Martin, Electroanalytical determination of diazinon: direct current and differential pulse polarography and adsorptive stripping voltammetry, Electroanalysis, 2(1990) 567-71.

[52] H. Bagheri, A. Afkhami, H. Khoshsafar, M. Rezaei, A. Shirzadmehr, Simultaneous electrochemical determination of heavy metals using a triphenylphosphine/MWCNTs composite carbon ionic liquid electrode, Sensors and Actuators B: Chemical, 186(2013) 451-60.

[53] H. Karimi-Maleh, F. Tahernejad-Javazmi, N. Atar, M. L. Yola, V.K. Gupta,.A.A. Ensafi, A novel DNA biosensor based on a pencil graphite electrode modified with polypyrrole/functionalized multiwalled carbon nanotubes for determination of 6-mercaptopurine anticancer drug, Industrial & Engineering Chemistry Research , 54 (2015) 3634-3639.

[54] V.K. Gupta, H. Karimi-Maleh, R. Sadegh, Simultaneous determination of hydroxylamine, phenol and sulfite in water and waste water samples using a voltammetric nanosensor, International Journal of Electrochemical Science, 10 (2015) 303-316.

[55] A. Afkhami, T. Madrakian, S.J. Sabounchei, M. Rezaei, S. Samiee, M. Pourshahbaz, Construction of a modified carbon paste electrode for the highly selective simultaneous

electrochemical determination of trace amounts of mercury (II) and cadmium (II), Sensors and Actuators B: Chemical, 161(2012) 542-8.

[56] M.R. Driss, M.C. Hennion, M.L. Bouguerraca, Determination of carbaryl and some organophosphorus pesticides in drinking water using on-line liquid chromatographic preconcentration techniques, Journal of Chromatography A, 639(1993) 352-8.

Authors biography

Niyoosha Pajooheshpour: is a MSC student at Faculty of Pharmaceutical Chemistry, Pharmaceutical Sciences Branch, Islamic Azad University. Her research interests include the development of electrochemical sensors for the detection of pharmaceutical species and environmental pollutants.

Mosayeb Rezaei received his MSc in Analytical Chemistry in 2011 at Bu-Ali Sina University, Hamedan, Iran. He is currently a researcher at electrochemical analysis.

Ali Hajian is a project assistant in the field of microsystem engineering at the Institute of Sensor and Actuator Systems (ISAS) in Vienna University of Technology, in Austria. Before, joining ISAS in August 2016, he worked as a scientific researcher at the Department of Microsystems Engineering (IMTEK) in the University of Freiburg in Germany for almost three years. His research is mainly focused on low temperature co-fired ceramics (LTCC) technology as well as electrochemistry including sensors and also energy storage and conversion.

Abbas Afkhami received his Ph.D. in Analytical Chemistry in 1991 at Shiraz University, Shiraz, Iran. He is currently a Professor of Analytical Chemistry at Bu-Ali Sina University, Hamedan, Iran. His research interest comprises the development of the new optical, chemical and electrochemical sensors for chemical and biological species.

Mika Sillanpää is a professor at the Lappeenranta University of Technology, Finland, and courtesy professor at the Florida International University, USA. He has over 20 years of expertise in green chemistry, analytical chemistry, and environmental engineering and has worked extensively with adsorption, photocatalysis, electrochemical treatment, and advanced oxidation processes as well as environmental analysis. Professor Sillanpää has published several books

and coauthored over 600 articles in peer-reviewed journals and international conference proceedings. He has also established close collaboration with over 80 research partners from the world's leading laboratories across six continents.

Fabiana Arduini is currently Senior Researcher at Department of Chemical Science and Technology (Analytical Chemistry), University of Rome Tor Vergata. Her research interests include the development of electrochemical sensors, Electrochemical Biosensors, Printed Electrodes, Paper-based printed sensors, sensor system modified with nanomaterials. She works on real applications in the field of environmental, food, and clinical analytical chemistry. Her research activity has been published in several papers

Hasan Bagheri is currently Associate Professor of Analytical Chemistry. His activities concerns the construction of different optical and electrochemical sensors/biosensors and their application in analytical matrices. His current research interests are in the field of fabrication of electrochemical sensors/biosensors and lateral flow kits based on new nanomaterials.

Figures caption

Scheme 1. (A) Synthesis of Au-Pt@BSA-GNRs bi-metallic nanoclusters and (B) preparation of the Au-Pt@BSA-GNRs/GCE biosensor.

Fig. 1 (a) UV-visible spectrum of Au-Pt@BSA (b) Fluorescence spectra of BSA, Pt@BSA, Au@BSA, and Au-Pt@BSA; (c) XRD of BSA, synthesized Au@BSA, Pt@BSA and Au-Pt@BSA; (d) FT-IR spectra of BSA, synthesized Au@BSA, Pt@BSA and Au-Pt@BSA-GNRs.

Fig. 2 (a) TEM image of Au-Pt@BSA; (b) EDX spectrum of Au-Pt@BSA.

Fig. 3 (a) CVs of GCE, BSA/GCE, BSA-GNRs/GCE, Au@BSA-GNRs/GCE, Pt@BSA-GNRs/GCE and Au-Pt@BSA-GNRs/GCE in 5 m K4[Fe(CN)6]$^{3-/4-}$ in 1.0 M KCl; (b) Nyquist plots of prepared electodes, (c) CVs of Au-Pt@BSA-GNRs/GCE at different scan rates from 50 to 1000 mVs^{-1} (Insets; plot of I *vs.* v$^{1/2}$ and E *vs.* Log v).

Fig. 4 (a) SWASVs of unmodified GCE, BSA/GCE, BSA-GNRs/GCE, Pt@BSA-GNRs/GCE, Au@BSA-GNRs/GCE, and Au-Pt@BSA-GNRs/GCE in the presence of 6.0 µM diazinon and Au-Pt@BSA-GNRs/GCE in the absence of the analyte; (b) SWASVs of 5.0 µM diazinon on Au-Pt@BSA-GNRs/GCE at different pHs from 1 to 8, (c) Plot of pH *vs.* I of 5.0 µM diazinon on Au-Pt@BSA-GNRs/GCE; (d) plot of pH *vs.* E of 5.0 µM diazinon on Au-Pt@BSA-GNRs/GCE; (f) effect of the deposition potential on the stripping peak current for 5.0 µM diazinon on Au-Pt@BSA-GNRs/GCE; and (e) effect of the accumulation time on the stripping peak current for 5.0 µM diazinon on Au-Pt@BSA-GNRs/GCE.

Fig. 5 (a) SWASVs of Au-Pt@BSA-GNRs/GCE at different concentrations of diazinon from 0.01 to 10.0 and 10 to 170 μM; (b) the corresponding calibration curves.

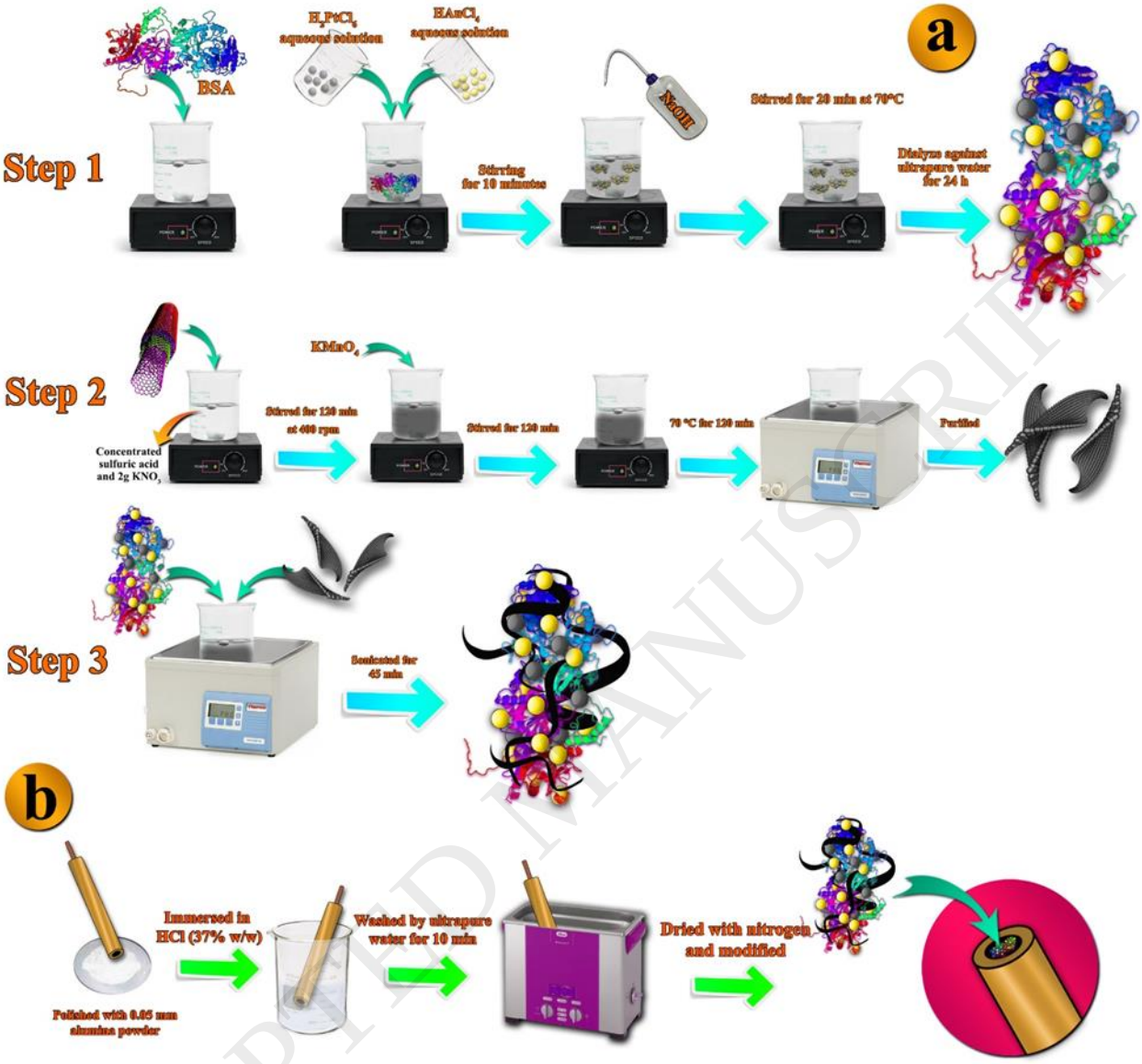

Scheme 1

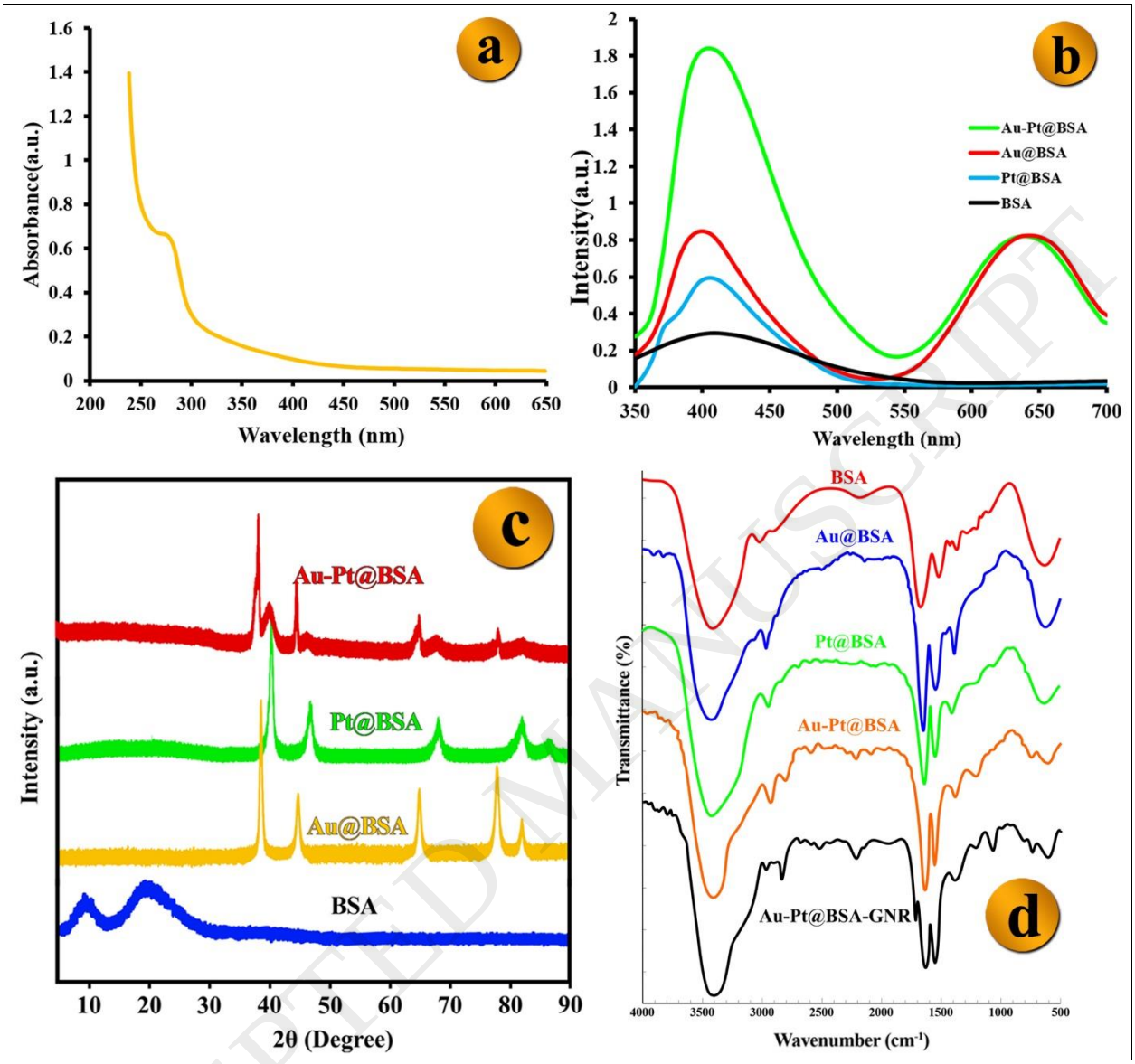

Fig. 1

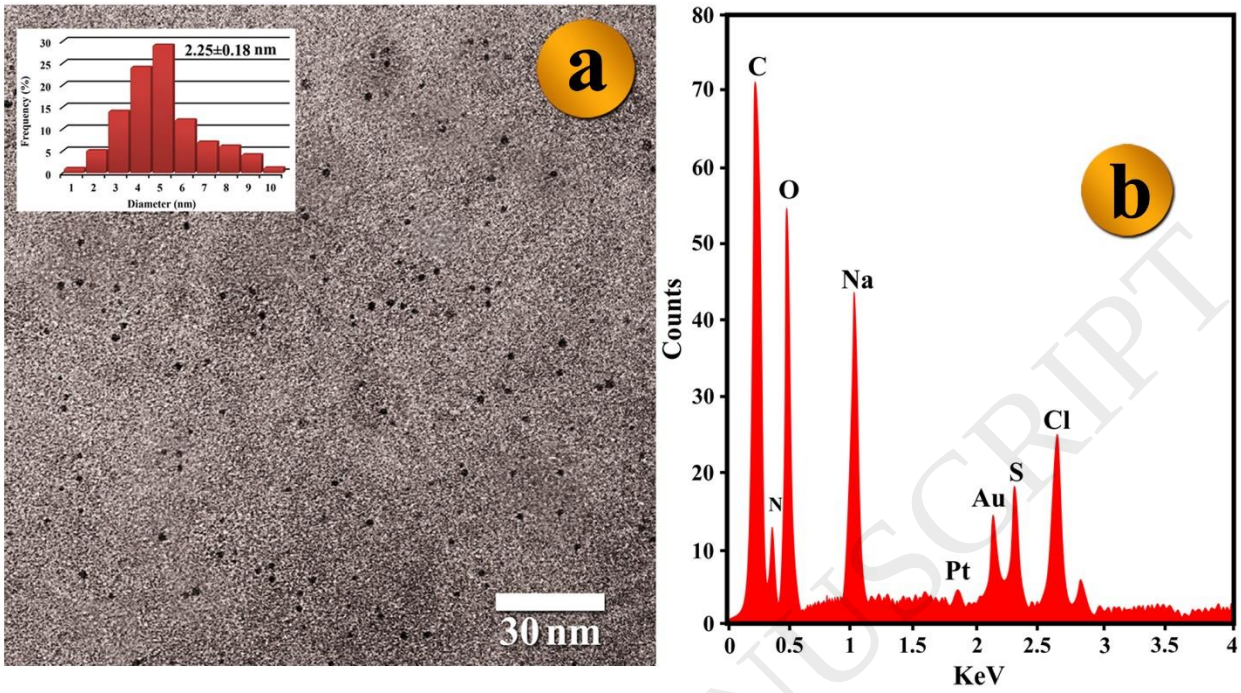

Fig. 2

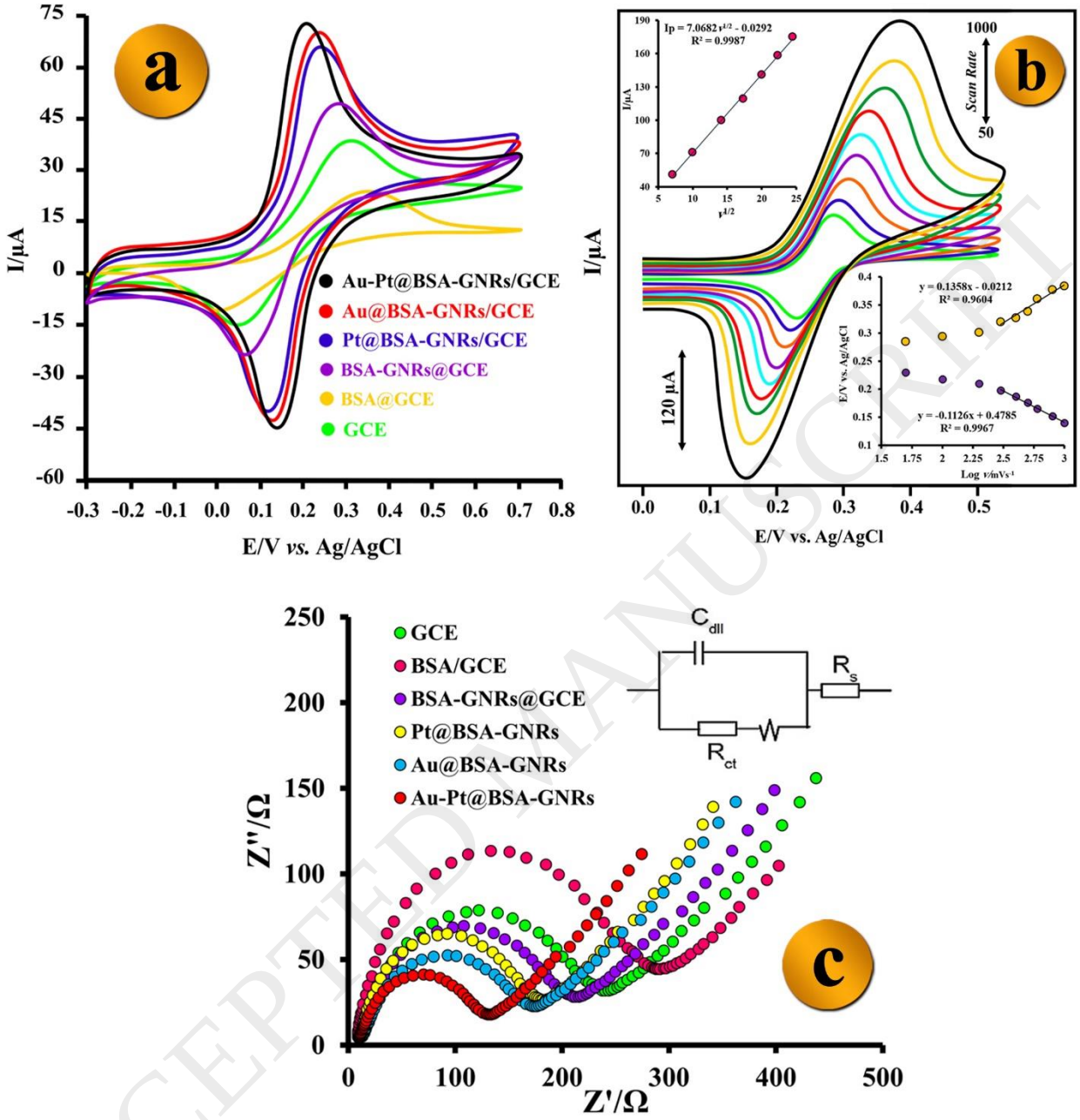

Fig. 3

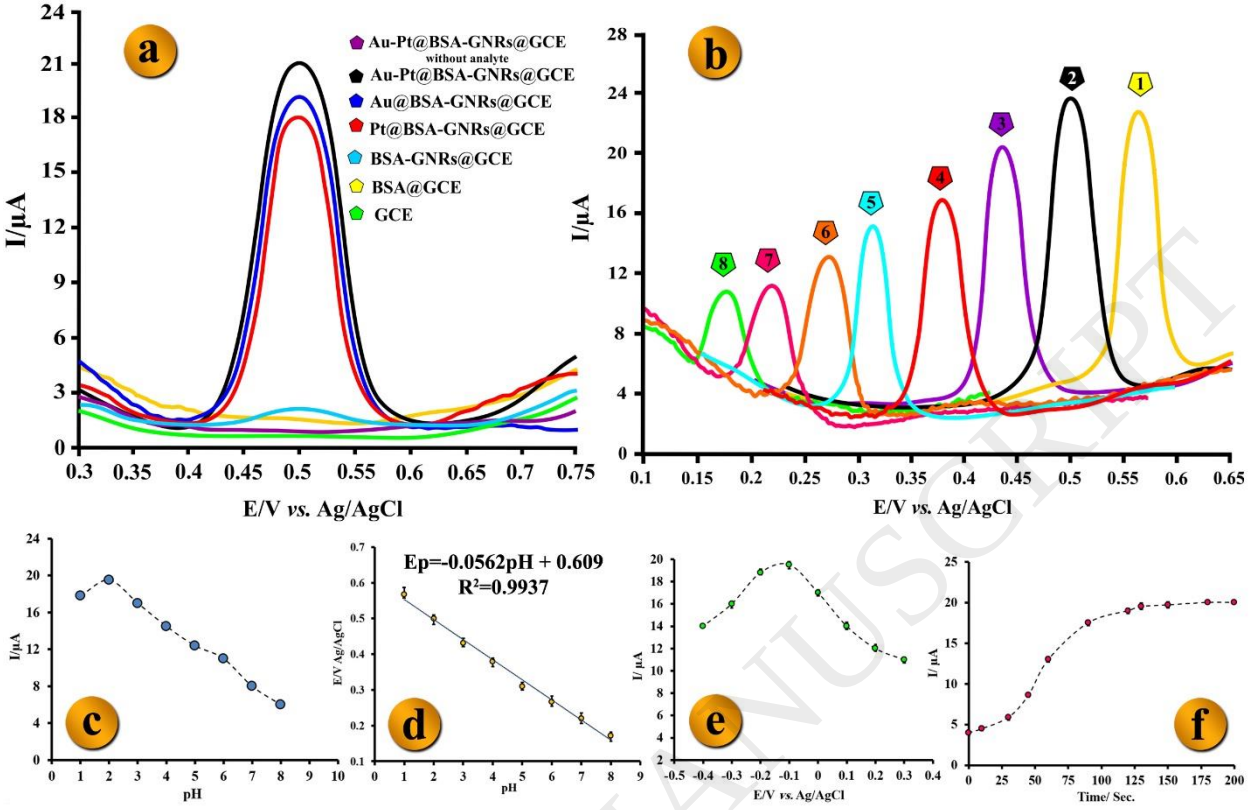

Fig. 4

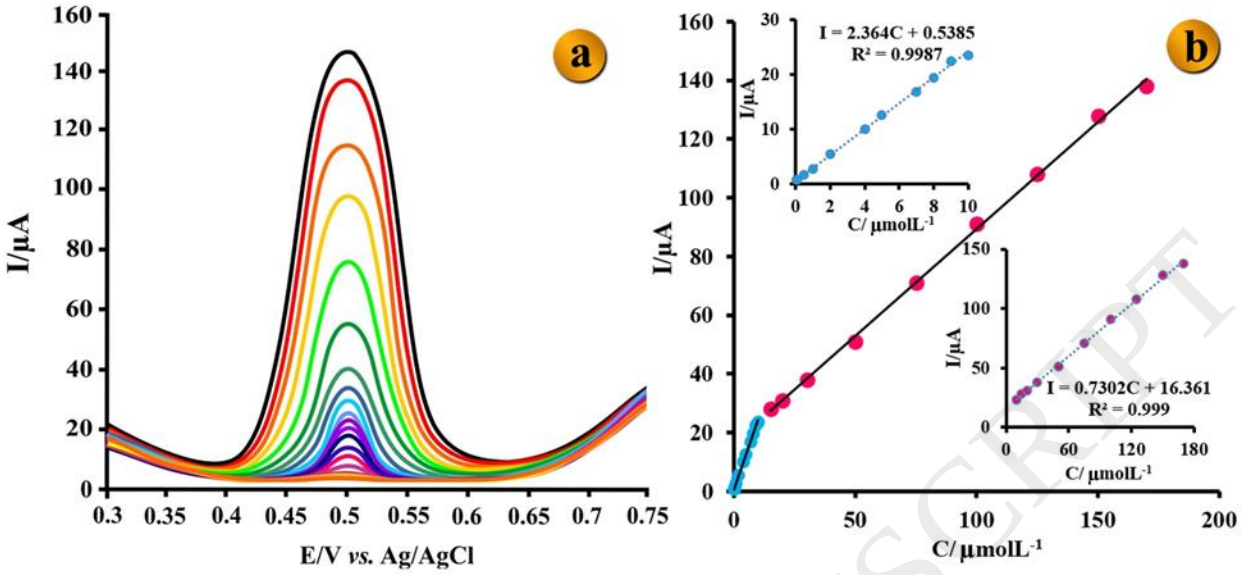

Fig. 5

Table 1. The determination results of diazinon in wastewater, river water, tap water, soil, apple, cucumber, carrot, tomato and lettuce samples (n = 3).

Samples	Added ($\mu molL^{-1}$)	Proposed Method ($\mu molL^{-1}$)	Recovery (%)	RP-HPLC/UV*
Waste water	1.00	1.02± 0.04	102.0	0.95 ± 0.05
	5.00	4.92 ± 0.12	98.4	4.94 ± 0.09
	10.00	10.11± 0.20	101.1	10.17± 0.21
River water	1.00	0.97 ± 0.04	97.0	1.04 ± 0.06
	5.00	4.96 ± 0.11	99.2	4.99 ± 0.08
	10.00	10.14± 0.18	101.4	10.11± 0.14
Tap water	1.00	1.02 ± 0.05	102.0	1.03 ± 0.05
	5.00	5.11 ± 0.13	102.2	5.08 ± 0.10
	10.00	9.89 ± 0.24	98.9	9.92 ± 0.14
Soil	1.00	1.05 ± 0.03	105.0	0.94 ± 0.07
	5.00	5.20 ± 0.31	104	5.15 ± 0.16
	10.00	9.75± 0.36	97.5	10.09± 0.18
Apple	1.00	0.96± 0.06	96.0	0.95± 0.07
	3.00	2.86 ± 0.21	95.3	2.82 ± 0.22
	5.00	5.12± 0.16	102.4	5.17± 0.25
Cucumber	1.00	1.04± 0.05	104.0	1.05± 0.08
	3.00	2.89 ± 0.20	96.3	2.93 ± 0.17
	5.00	5.12± 0.15	102.4	4.90± 0.24
Carrot	1.00	1.01± 0.05	101.0	1.03± 0.06
	3.00	3.15 ± 0.14	105.0	3.14 ± 0.22
	5.00	4.79± 0.24	95.8	4.88± 0.29
Tomato	1.00	1.01± 0.06	101.0	0.96± 0.08
	3.00	3.04 ± 0.08	101.3	3.06 ± 0.06
	5.00	5.24± 0.31	104.8	5.13± 0.26
Lettuce	1.00	0.96± 0.05	96.0	1.04± 0.05
	3.00	2.86 ± 0.19	95.3	2.96 ± 0.17
	5.00	5.21± 0.25	104.2	5.19± 0.28

* Preconcentration onto 5 µm C_{18}-silicaor 7 µm polystyrene-divinyl benzene co-polymer with subsequent backflushonto analytical HPLC column. Sample volume up to 300 mL and UV wavelength of determination 254 mn [56].